

# Analytic insight into shear-wave AVO for fractured reservoirs

Andreas Rüger

*Department of Geophysics*

*Center for Wave Phenomena*

*Colorado School of Mines, Golden, CO 80401, USA*

## ABSTRACT

It is well established that azimuthal anisotropy caused by fracture systems in reservoir rocks has a first-order influence on kinematic properties of shear waves. Analysis of time differences between split shear waves at near-vertical incidence can yield information on the orientation of the crack system and estimates of crack density. However, this technique may have a limited vertical resolution and may not be usable if the reservoir is too thin to generate measurable time delays.

Study of the normal-incidence reflection coefficients of the two split shear modes can be used to overcome this difficulty. Here, extensions to shear-wave amplitude variation with offset (AVO) analysis are investigated using concise linearized reflection coefficients in the two vertical symmetry planes of azimuthally anisotropic media. The derived approximations explicitly describe the influence of medium parameters on the AVO gradients and the higher angle terms of the shear-wave reflection coefficients. The contribution of anisotropy in the subsurface is hereby characterized by the shear-wave splitting parameter  $\gamma$  and anisotropy parameters similar to Thomsen's (1986) coefficients.

The important result of this study is that AVO gradients of shear waves propagating in the vertical symmetry planes of fractured media are sensitive to the shear-wave splitting parameter and to parameter combination  $(\epsilon^{(V)} - \delta^{(V)})$  important for time processing in anisotropic media. Analytic insight developed in this study naturally leads to an inversion algorithm for the isotropy and anisotropy parameters of the fractured medium.

**Key words:** AVO, shear waves, anisotropy, HTI media

## Introduction

Shear-wave surveys are routinely acquired and interpreted for the presence of azimuthal anisotropy (Michelena, 1995; Lynn, 1995; Kendall, 1995). The main objective of these studies is to relate the anisotropy (determined by conventional shear-wave splitting analysis) to the fracture parameters of the medium. Anisotropic compressional stresses required to fracture rocks are relatively small and even flat-lying strata are commonly fractured, with the most famous example probably being the Austin Chalk in Texas (Mueller, 1991).

Although natural fractures can occur in many forms and settings, depending on the orientation and the mag-

nitude of paleo- and current stress regimes, the most plausible reason for the observed anisotropy is the presence of aligned cracks in an isotropic matrix (Crampin, 1985; Crampin & Atkinson, 1985). A first-order model that describes the presence of vertical stress-aligned cracks is the transversely isotropic medium with a horizontal axis of symmetry (HTI) (Thomsen, 1988). Most of the derivations and insights developed in this paper are restricted to HTI models, but extensions of this work to orthorhombic symmetry systems are discussed and presented in more detail in Rüger (1996b).

Azimuthal anisotropy has a first-order influence on vertically incident shear waves causing them to be split

into two components traveling with different velocities. The parameter of crack systems of great interest in exploration is the crack density, which is approximated by the fractional difference between the velocities of split shear waves at vertical incidence [Thomsen's (1986) coefficient  $\gamma$ ]. Estimates of anisotropy using the time delay between the fast and slow shear waves yield robust measurements of  $\gamma$  averaged over the propagation path of the shear waves within the medium. Thus, analysis of shear-wave kinematic signatures via the classical rotation analysis (Alford, 1986) helps to estimate the crack density (for HTI media), albeit with a low vertical resolution.

For situations where a detailed measure of local anisotropy (highly resolved in depth/time) is desired, or where the rotation analysis fails due to insignificant time delays, Thomsen (1988), Lynn and Thomsen (1990) and Yardley et. al. (1991) suggest using the differences in normal-incidence reflection coefficients and the amplitude-variation-with-offset signature between the fast and slow shear waves to characterize the target horizon.

The reflection response of plane waves at interfaces between anisotropic media has been thoroughly investigated in the literature (Musgrave, 1970; Henneke, 1972; Keith & Crampin, 1977). The computation of the reflection coefficient is straightforward and generally requires a numerical inversion of a 6x6 matrix. The entries of the matrix include polarizations and tractions of three different wave modes in both media that have to be obtained by the eigenvector analysis of the Christoffel equation.

Yardley et. al. (1991) used the reflectivity method to compute the reflection coefficients as a function of incidence angle for various azimuthally anisotropic two-layer models. In their studies, they modeled layers of HTI symmetry that contain parallel vertical cracks normal and oblique to the survey line. They qualitatively described and discussed changes of the reflection response for layers with water- and gas-filled cracks and observed a dependence of the AVO response on both the crack density and crack content. Yardley et. al. (1991) also emphasized severe difficulties in measuring shear-wave amplitudes if the acquisition (survey) line is not parallel or perpendicular to the crack orientation.

The results obtained by Yardley et. al. (1991) motivate a more detailed analysis of the AVO problem for shear waves in HTI media. To overcome the algebraic complexity of the reflection/transmission problem in anisotropic media, I hereby follow the approach devised by Richards and Frasier (1976), Aki and Richard (1980) and Shuey (1985) for isotropic media to derive concise analytic approximations of the reflection and transmission coefficients. The resulting equations, which are linear in

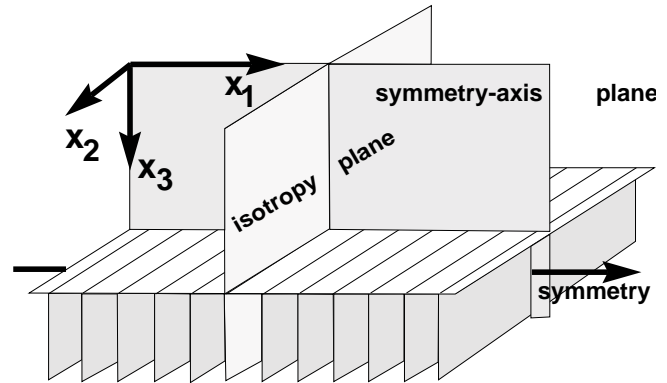


**Figure 1.** Sketch of an HTI model. The model has two vertical symmetry planes: the isotropy plane and the symmetry-axis plane.

the relative changes of the elastic parameters across the reflecting boundary, reveal the dependence of the normal incidence reflection coefficient and the AVO gradient on the anisotropy in the medium.

The analytic equations for shear-wave reflection coefficients derived in this paper are valid for small changes in the elastic properties across interfaces between isotropic and HTI layers. The solutions are also valid for interfaces between two HTI media if the principal axes of symmetry coincide in both layers and for interfaces between HTI layers and transversely isotropic layers with a vertical axis of symmetry (VTI). A typical geologic model for the VTI/HTI boundary is a massive shale layer overlying a fractured reservoir. In all situations described in the paper, the survey line has to be either near-parallel or near-perpendicular to the crack orientation. The orientation of the symmetry axis can be obtained in many exploration contexts by in-situ stress measurements (Lynn & Thomsen, 1990), wireline data, geologic studies and  $P$ -wave AVO and NMO analysis (Rüger, 1996a; Rüger & Tsankin, 1995). If the incidence and symmetry planes do not coincide, three wave modes are coupled and the polarization of the individual wave modes is more complicated, hampering a reliable extraction of the amplitudes.

Models with horizontal transverse isotropy represent simple first-order approximations of fractured media. Extension of this work to subsurfaces with (more complicated and more realistic) orthorhombic symmetry systems is briefly discussed.

## Shear-wave propagation in HTI media

Wave propagation in anisotropic media is a complex physical phenomenon. Before discussing the feasibility of fracture characterization using dynamic signatures of

shear waves, it is useful to recall basic properties of waves propagating in HTI media and introduce notation. Let us assume that the symmetry axis of the HTI model is parallel to the  $x_1$  direction (Figure 1). The  $[x_1, x_3]$ -plane that contains the symmetry axis is hereafter referred to as the “symmetry-axis plane.” Waves confined to the plane normal to the symmetry axis have the same velocity for all incidence angles; hence, this plane is the so-called “isotropy plane” or “fracture plane.”

Analysis of seismic waves (Červený, 1972) shows that for a given slowness, three plane-wave modes with mutually orthogonal polarizations can propagate in anisotropic media. If the medium is HTI, one mode ( $S^{\parallel}$ ) is polarized within the isotropy plane (the  $[x_2, x_3]$  plane). This mode is truly transverse since it is polarized perpendicular to the propagation direction. The two remaining modes have quasi-longitudinal ( $qP$ ) and quasi-transverse ( $S^{\perp}$ ) polarizations with respect to the slowness direction  $p$  (see Figure 2). Polarization directions are defined according to the convention in Aki and Richards (1980): the positive polarization direction is such that the horizontal component points in the direction of horizontal slowness.

The minimum values of the phase velocities for the  $S^{\parallel}$  and  $qP$  mode are in the symmetry direction ( $x_1$  axis), while the maximum occurs in the isotropy plane. By contrast, the  $S^{\perp}$ -shear mode must exhibit at least one extremum as the propagation direction changes from the symmetry-axis directions towards the isotropy plane because the  $S^{\perp}$  phase velocity is identical in both directions. Unlike the  $S^{\parallel}$  and  $qP$  modes, the  $S^{\perp}$  wave may exhibit triplicated wavefronts even in homogeneous anisotropic media. Illustrations and qualitative description of wavefront triplications can be found, for example, in Rüger (1994).

The discussion in this paper is mainly focused on the reflections of shear waves traveling in the two vertical symmetry planes of HTI models. Figures 3a and 3b illustrate how  $S^{\parallel}$  and  $S^{\perp}$  waves propagate within the isotropy plane and reflect from the interface. The HTI medium has a vertical  $P$ -wave velocity  $V_{P0} = 2.6$  km/s and a vertical shear velocity  $V_{S0} = 2$  km/s. The anisotropy simulated in this model is described by generic Thomsen’s (1986) parameters  $\epsilon = 0.15$ ,  $\delta = -0.1$  and  $\gamma = 0.1$ . The black lines emitted from the source at the origin denote seismic rays. The continuous white lines are obtained by simply connecting points of 1s traveltime of the individual rays and thus represent wavefronts. The  $S^{\perp}$  mode shows a perfectly circular wavefront typical for isotropic wave propagation. As expected, the  $S^{\parallel}$  wavefront is also circular, but it is more advanced than the  $S^{\perp}$  wavefront and already reflects from the interface. The different speed of the two shear waves is a manifestation

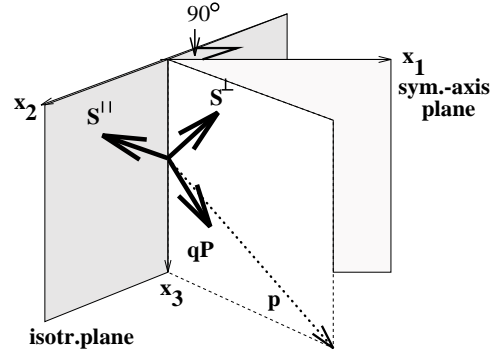


**Figure 2.** Three modes ( $S^{\parallel}$ ,  $S^{\perp}$ ,  $qP$ ) with mutually orthogonal polarization vectors are traveling in anisotropic media. For HTI media, the polarization vector of the  $S^{\parallel}$  wave is confined to the isotropy plane and is always perpendicular to the slowness direction  $p$ .

of the well-known phenomenon of shear-wave splitting that indicates that the subsurface model is *not* isotropic.

Rays and wavefronts of shear waves propagating within the symmetry-axis plane are shown in Figures 3c ( $S^{\parallel}$ ) and 3d ( $S^{\perp}$  mode). For near-vertical propagation, the  $S^{\parallel}$  wavefront is more advanced than that of the  $S^{\perp}$  wave. Additionally, a closer view at the figures reveals that several features of these figures differ significantly from the familiar behavior of rays and wavefronts in isotropic homogeneous media:

- The wavefronts are not circular. In particular, the  $S^{\parallel}$ -wavefront is most advanced in vertical direction. This can be seen by comparison with the circular  $S^{\parallel}$ -wavefront in the isotropy plane (Figure 3a): Both wavefronts coincide at vertical incidence, but the symmetry-axis plane  $S^{\parallel}$ -wavefront is less advanced for large incidence angles.
- The  $S^{\perp}$ -wavefront clearly shows an unusual angular shape although the medium is homogeneous.
- The ray density is not uniform. Moreover, the angular distribution of ray density differs for  $S^{\parallel}$ - and  $S^{\perp}$ -waves. While the  $S^{\parallel}$ -wave shows a uniform ray-distribution, a concentration of  $S^{\perp}$ -rays is seen for ray angles of about  $45^{\circ}$ .

Figures 3a-d also demonstrate the dynamic properties of the wavefields. More specifically, the ray density is related to the phenomena of energy focusing and defocusing (Tsvankin & Chesnokov, 1990; Tsvankin, 1995). Energy increases in regions with a high concentration of rays (or, equivalently, a high concentration of group velocity vectors). Conversely, a low concentration of rays indicates energy defocusing. This phenomenon needs to be taken into account for reliable AVO analysis in anisotropic media (Tsvankin, 1995). Variations of amplitudes

with offset are not only caused by the changes in the reflection coefficients with angle, but also by focusing and defocusing of energy during the wave-propagation in the anisotropic overburden. After deriving equations for reflection coefficients in HTI media, I therefore first consider the simpler case of an isotropic layer overlying a fractured layer. In this case, the wave-propagation effects are limited to spherical divergence of energy. The more complex case of an HTI layer overlying an isotropic layer or the contact between two anisotropic layers is discussed later in the text.

### Linearized reflection coefficients

Physical constraints on the continuity of the displacement and traction between layers in welded contact yield a system of equations that can be solved for the reflection and transmission coefficients. Depending on the type of symmetry above and below the interface and the incident-wave mode, two, four or six boundary conditions have to be solved for the amplitude coefficients of the reflected and transmitted waves.

Mathematically, the equation to be solved can be expressed as

$$\mathbf{A} \mathbf{R} = \mathbf{b}, \quad (1)$$

where  $\mathbf{A}$  is the boundary equation matrix formed by the scattered (reflected and transmitted) waves,  $\mathbf{R}$  is the vector of reflection and transmission coefficients, and  $\mathbf{b}$  is composed of the contribution of the incident wave to the boundary conditions (Aki & Richards, 1980; Thomsen, 1993).

Solutions for the plane-wave reflection and transmission coefficients are algebraically very involved and require an inversion of the boundary matrix  $\mathbf{A}$ . The complexity of the energy-partitioning problem at planar interfaces obscures any insight into the dependence of the reflection coefficient on the medium parameters and incidence angle. To overcome this difficulty, I follow Richards and Frasier (1976) and Aki and Richards (1980) approach of linearizing the reflection coefficient with respect to relative changes in elastic parameters across the interface. Extensions of this approach to AVO-analysis have been developed by Shuey (1985) and Wright (1986) (for isotropic media) and for transversely isotropy media by Banik (1987), Thomsen (1993) and Rüger (1996a). In most exploration contexts, the two layers under consideration have similar properties and it is convenient to express the elastic properties as functions of the average values and relative differences in the model parameters. The densities in the upper and lower layer, for example, can be written as functions of the average density

$\bar{\rho} = 1/2(\rho_2 + \rho_1)$  and the difference  $\Delta\rho = \rho_2 - \rho_1$ :

$$\begin{aligned} \rho_1 &= \bar{\rho} \left(1 - \frac{1}{2} \frac{\Delta\rho}{\bar{\rho}}\right), \\ \rho_2 &= \bar{\rho} \left(1 + \frac{1}{2} \frac{\Delta\rho}{\bar{\rho}}\right). \end{aligned}$$

Analogous expressions are defined for the shear and compressional velocities  $\beta$  and  $\alpha$ , respectively.

### Isotropic layers

For isotropic layers, the solution for  $\mathbf{R}$  in equation (1), linearized with respect to small elastic contrast coefficients is fairly straightforward (Thomsen, 1993). The approximate (linearized) reflection coefficient for the mode polarized perpendicular to the vertical propagation plane (here denoted as the *SH*-mode to follow the standard notation), for example, yields

$$\begin{aligned} R_{SH}^{\text{iso}} &= -1/2 \left( \frac{\Delta\rho}{\bar{\rho}} + \frac{\Delta\beta}{\bar{\beta}} \right) + 1/2 \frac{\Delta\beta}{\bar{\beta}} \sin^2 j + \\ &1/2 \frac{\Delta\beta}{\bar{\beta}} \sin^2 j \tan^2 j, \end{aligned} \quad (2)$$

or, equivalently

$$R_{SH}^{\text{iso}} = -1/2 \left( \frac{\Delta\rho}{\bar{\rho}} + \frac{\Delta\beta}{\bar{\beta}} \right) + 1/2 \frac{\Delta\beta}{\bar{\beta}} \tan^2 j, \quad (3)$$

with  $j$  denoting the incidence shear-wave angle. The disadvantage of this equation is that the approximation is not exact for normal incidence. Differences between vertical incidence reflection coefficients of different wave modes will later be attributed to (small) anisotropic parameters and any inaccuracy due to the isotropic approximation can hamper the analysis and inversion for anisotropy coefficients. I therefore suggest to introduce the shear-wave impedance  $Z = \rho\beta$  and to use the exact normal-incidence reflection coefficient:

$$R_{SH}^{\text{iso}} = -1/2 \frac{\Delta Z}{\bar{Z}} + 1/2 \frac{\Delta\beta}{\bar{\beta}} \tan^2 j. \quad (4)$$

From the physical point of view, it is clear that the normal-incidence reflection coefficient at isotropic boundaries is the same for all shear-modes because the polarization vector is always parallel to the reflecting interface. For oblique incidence angles, *SV* waves will generate reflected and transmitted *P*-waves in addition to shear waves and it is not surprising that the angular variation of the *SV* reflection coefficient differs from that in equation (4) (Thomsen, 1988; Thomsen, 1993):

$$\begin{aligned} R_{SV}^{\text{iso}} &= -1/2 \frac{\Delta Z}{\bar{Z}} + \left( \frac{7}{2} \frac{\Delta\beta}{\bar{\beta}} + 2 \frac{\Delta\rho}{\bar{\rho}} \right) \sin^2 j - \\ &1/2 \frac{\Delta\beta}{\bar{\beta}} \sin^2 j \tan^2 j. \end{aligned} \quad (5)$$

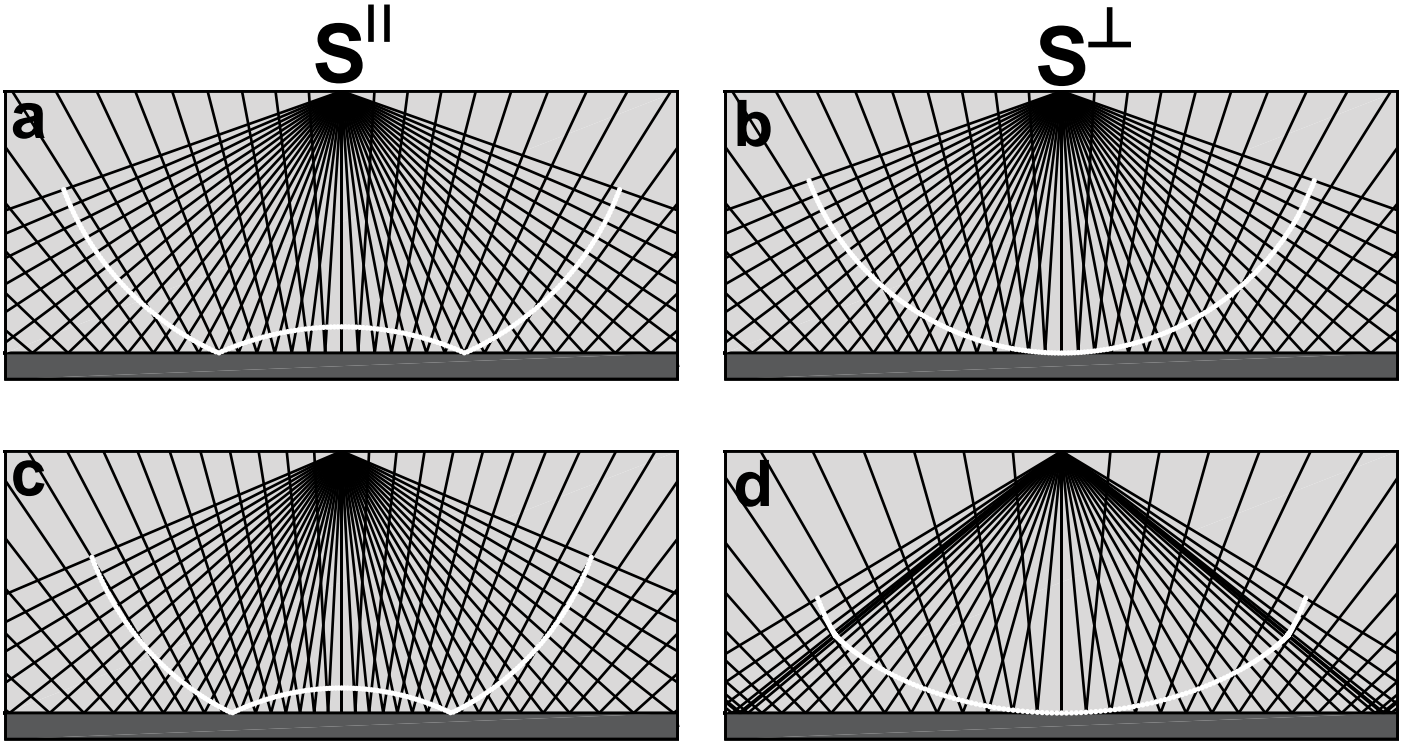


**Figure 3.** Propagation and reflection of shear waves traveling within the two vertical symmetry planes of an HTI medium ( $V_{P0} = 2.6\text{km/s}$ ,  $V_{S0} = 2\text{km/s}$ ,  $\epsilon = 0.15$ ,  $\delta = -0.1$ ,  $\gamma = 0.1$ ). **a.**) and **b.**) show  $S^{\parallel}$  and  $S^{\perp}$  waves propagating in the isotropy plane, respectively; **c.**) and **d.**) denote  $S^{\parallel}$  and  $S^{\perp}$  waves traveling in the symmetry-axis plane. Shown in black are the seismic raypaths, the white curves denote the wavefronts at 1s traveltime.

It is well known that the coupling between transverse and longitudinal waves for oblique incidence angles manifests itself in the dependence of the  $P$ -wave AVO gradient on the shear-wave velocity (Shuey, 1985). Surprisingly, the opposite is not the case and the  $SV$ -wave AVO gradient is independent of  $\frac{\Delta\alpha}{\alpha}$  under the assumption of small relative changes in the elastic parameters across the reflecting boundary\*.

Equation (5), as well as most reflection-coefficient approximations in this paper, show a simple decomposition of the form

$$R(j) = A + B \sin^2 j + C \sin^2 j \tan^2 j . \quad (6)$$

The advantage of representing the reflection coefficient in this form has been thoroughly discussed in the literature (Castagna & Backus, 1993). Here it is appropriate to make some observations for the particular case of shear-

wave amplitude studies. The normal-incidence term  $A$ , for example, can hardly be obtained because of the difficulty to extract absolute amplitudes in data processing. However, as observed by Thomsen (1988) and Lynn and Thomsen (1990), comparison of  $A$  for both shear modes in models of HTI symmetry can yield valuable insight into medium parameters.

The AVO-gradient term  $B$  is of most interest in conventional  $P$ -wave AVO studies, as well as in shear-wave amplitude-variation-with-offset analysis. Note that this term dominates the angular variation in the reflection response for small angles of incidence ( $< 30^\circ$ ) recorded in most seismic surveys. Small incidence angles are particularly important for shear-wave studies because the first critical angle is often small. Even moderate incidence angles of about  $30^\circ$  can generate evanescent energy at the free surface that induces complicated phase and amplitude distortions. Thus, for shear waves, it is often difficult to obtain reliable estimates of the  $C$ -term in equation (6).

\* The approximate  $P$ - $P$ -transmission coefficient is also independent of  $\frac{\Delta\beta}{\beta}$ . Apparently,  $P$ -wave AVO is based on a rare physical gratitude.

The simplicity of the linearized equations helps to quickly identify the contributions of different physical parameters to the reflection response. For instance, we are reminded that only relative differences in elastic parameters influence the reflected seismic signature. For the particular case of the *SH* reflection coefficient, equation (3) shows that the relative differences in density and shear-wave velocity have the same influence on the normal-incidence reflection coefficient. Additionally, we recognize that  $\frac{\Delta\beta}{\beta}$  is the only term responsible for small- and large-angle variations of the *SH*-wave reflection response. Thus, if amplitudes of *SH*-waves incident at large angles ( $> 20^\circ$ ) can be reliably recovered, it is advantageous to plot them as a function of the squared tangent of the incidence angle [see equation (3)].

### Vertical transverse isotropy

The first step away from simple, isotropic media is to consider vertical transverse isotropy (VTI), the symmetry system that can be caused by massive shales and thinly-layered media. The three wave modes propagating in VTI media are the quasi *P* wave, the quasi *SV* wave and the truly transverse *SH* wave. Velocities in transversely isotropic media depend on the angle with the symmetry axis and every velocity parameter needs to be associated with a certain propagation direction. In the following, shear-wave velocity  $\beta$  is the vertical shear-velocity which is identical for both shear modes in VTI media; the compressional velocity  $\alpha$  in the equations below also correspond to vertical incidence. Seismic signatures in VTI media are invariant with respect to rotations about the vertical symmetry axis; however, while for VTI media the reflection response is still *azimuthally* invariant, the variation in velocity for different angles with vertical has an impact on the angular variation of the reflection coefficient.

Thomsen's (1986) anisotropy parameters can be used to describe the departure from isotropy. Using  $\delta_1, \epsilon_1, \gamma_1$  and  $\delta_2, \epsilon_2, \gamma_2$  to describe the anisotropy in the first and second layer, it is possible to derive linearized reflection coefficients (Thomsen, 1993; Rüger, 1996a) for VTI media by adding the appropriate anisotropic contributions to equations (4) and (5). The reflection coefficient for the *SH* mode, for example, can be written as

$$R_{SH}^{VTI} = R_{SH}^{iso} + 1/2 (\gamma_2 - \gamma_1) \tan^2 j, \quad (7)$$

where  $j$  is the incident *phase* angle. As seen in equation (7), anisotropy contributes to the angular variation of the reflection coefficient. Ignoring the presence of anisotropy yields an erroneous AVO interpretation whenever there exists a difference between the anisotropy

parameters  $\gamma_1$  and  $\gamma_2$ . Finally, as for the isotropic AVO-contribution present in the expression for  $R_{SH}^{iso}$ , just one parameter ( $\gamma$ ) is responsible for small and large-angle variations caused by the vertical transverse isotropy.

The *SH*-phase velocity in VTI media (Thomsen, 1986) displays a similar  $\sin^2 j$ -term multiplied by the anisotropy parameter  $\gamma$  as the  $R_{SH}^{VTI}$  reflection coefficient. In the limit of weak anisotropy, the angular variation of the *SV*-wave phase velocity<sup>†</sup> is governed by  $\sigma = \left(\frac{\alpha}{\beta}\right)^2 (\epsilon - \delta)$  (Tsvankin & Thomsen, 1994) and it is not surprising that the parameter  $\sigma$  also appears in the approximate reflection coefficient for the *SV* wave:

$$R_{SV}^{VTI} = R_{SV}^{iso} + 1/2 \left(\frac{\bar{\alpha}}{\beta}\right)^2 (\epsilon_2 - \epsilon_1 + \delta_1 - \delta_2) \sin^2 j. \quad (8)$$

Unlike the isotropic *SV*-wave AVO gradient, equation (8) depends on the average compressional velocity. For a typical ratio of  $\bar{\alpha}/\beta \approx 2$ , the difference in  $(\epsilon - \delta)$  is of the same importance to the AVO gradient as the relative difference in density and vertical shear velocity [recall equation (5) for the dependence of  $R_{SV}^{iso}$  on  $\frac{\Delta\rho}{\rho}$  and  $\frac{\Delta\beta}{\beta}$ ]. For large angles of incidence and nonzero values of  $\frac{\Delta\beta}{\beta}$ , the  $\sin^2 \tan^2$ -term in  $R_{SV}^{iso}$  will give an increasingly important contribution to  $R_{SV}^{VTI}$ . Note that there is no similar large-angle term in the anisotropic addition in equation (8).

As discussed in Tsvankin and Thomsen (1994) and Tsvankin (1995), the same  $\left(\frac{\alpha}{\beta}\right)^2 (\epsilon - \delta)$ -term dominates the radiation pattern of *SV*-waves in VTI media and needs to be accounted for in AVO analysis.

### Horizontal transverse isotropy

The reflection coefficients for isotropic and VTI subsurface models are essentially known from previously published equations (Aki & Richards, 1980; Thomsen, 1993), although the specific form used in this paper was helpful in elucidating the physics of the energy-partitioning problem of shear waves. By contrast, azimuthally varying shear-wave AVO signatures for models of HTI symmetry have not yet been analyzed analytically and a few published studies have been based entirely on numerical experiments. Clearly, without an understanding of the relations between the medium parameters and the AVO response, it is hardly possible to make quantitative estimates of the influence of anisotropy on the recorded seismic signatures and, even more importantly, develop inversion procedures similar to conventional isotropic AVO analysis. Although the additional dependence on azimuth

<sup>†</sup> As discussed above, this shear-wave and the compressional wave are not truly transverse and longitudinal in VTI and HTI media, but I omit the qualifier *quasi* for brevity.

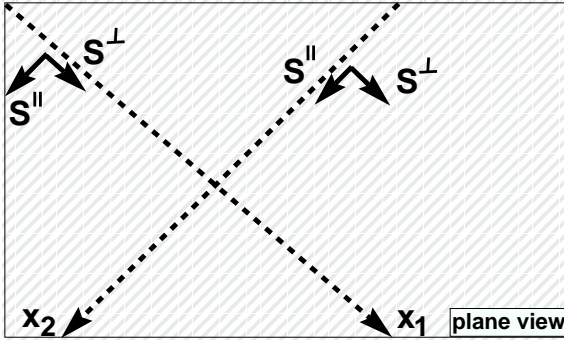


**Figure 4.** Sketch of a shear-wave experiment in the presence of aligned near-vertical cracks (plane view). Arrows show the polarization directions for  $S^{\parallel}$  and  $S^{\perp}$  waves. Amplitude analysis will be carried out along the strike ( $x_2$ ) and the symmetry-axis direction ( $x_1$ ).

makes the HTI reflection problem more involved, it can also yield more information about the anisotropy of the subsurface. Thus, it is reasonable to investigate the viability of extracting the subsurface parameters from the azimuthally-dependent shear-wave AVO response in HTI media.

### Strike-line survey

The survey geometry in Figure 4 is similar to that of shear-wave experiments by Lynn and Thomsen (1990) and Lynn et al. (1995). As described in the previous chapter, the  $S^{\parallel}$ -wave polarization is confined to the fracture plane (or isotropy plane) whereas the  $S^{\perp}$  wave is polarized perpendicular to it. Let us first consider an AVO experiment carried out along the fracture strike. It is hereby assumed that both layers are fractured in the same direction, but with different fracture intensity. If the source is oriented in the strike direction, a  $S^{\parallel}$  shear wave polarized within the fracture plane is generated. Within this plane, the shear-wave velocity is independent of the propagation angle and the approximate reflection coefficient is identical to the isotropic reflection coefficient for shear waves polarized within the propagation plane:

$$R_{S^{\parallel}}^{\text{strike}} = R_{SV}^{\text{iso}}, \quad (9)$$

with  $\alpha$  and  $\beta$  in  $R_{SV}^{\text{iso}}$  replaced by

$$\begin{aligned} \alpha &= \sqrt{\frac{c_{33}}{\rho}} \\ \beta &= \sqrt{\frac{c_{44}}{\rho}}, \end{aligned} \quad (10)$$

i.e., the compressional and shear velocities of waves polarized within the fracture plane.

For a survey aligned with fracture strike, the  $S^{\perp}$  wave is polarized perpendicular to the vertical propagation plane. Therefore, the corresponding approximate reflection coefficient has the form of equation (4):

$$R_{S^{\perp}}^{\text{strike}} = R_{SH}^{\text{iso}}, \quad (11)$$

where  $\beta$  in  $R_{SH}^{\text{iso}}$  needs to be replaced by the correct shear velocity  $\beta^{\perp}$ . The latter can be expressed as:

$$\beta^{\perp} = \sqrt{\frac{c_{55}}{\rho}}. \quad (12)$$

Sample computations of exact and approximate reflection coefficients of shear waves propagating in the isotropy plane are shown in Figure 5. In this experiment, the upper medium is isotropic. The parameters of the lower medium are equivalent to the coefficients for a saturated, fractured model ( $\gamma = 0.115$ ) shown in Thomsen (1995), Table 1. In this experiment, a relative change of 20 percent in the vertical compressional velocity, vertical  $S^{\parallel}$ -wave velocity and density across the reflecting boundary are assumed. The approximate  $S^{\parallel}$  reflection coefficient is shown in Figure 5a, together with the exact solution. Small deviations from the exact solution can be observed only for incident angles close to  $20^\circ$ . Figure 5b shows the exact  $S^{\perp}$  reflection response and the approximations using equations (2) and (4). The former approximation is slightly shifted vertically with respect to the exact solution due to the approximate normal-incidence term. Equation (4), on the other hand, is exact for vertical incidence. To enable a better comparison between gradient and intercepts of the two AVO responses, both  $S^{\perp}$  and  $S^{\parallel}$  reflection coefficients are combined in Figure 5c.

Differences in slope and normal incidence terms can be easily explained using the insight developed in the above discussion: The  $R_{S^{\parallel}}^{\text{strike}}$  normal-incidence term is more negative as compared to the  $S^{\perp}$  coefficient due to the larger shear-wave impedance contrast ( $\rho\beta > \rho\beta^{\perp}$ ). The  $R_{S^{\parallel}}^{\text{strike}}$  gradient, on the other hand, is influenced by two times the sum of relative changes in  $\beta$  and  $\rho$  as compared to  $1/2 \frac{\Delta\beta^{\perp}}{\beta^{\perp}}$  in the  $R_{S^{\perp}}^{\text{strike}}$  gradient.

What if anisotropy is ignored and both shear waves travel with the same velocities  $\beta$  in the lower medium? Certainly, both reflection coefficients are also different in the isotropic case, however, we would have missed the difference in normal-incidence reflection coefficient and the  $R_{S^{\perp}}^{\text{strike}}$  gradient is overestimated because  $\frac{\Delta\beta}{\beta} > \frac{\Delta\beta^{\perp}}{\beta^{\perp}}$ .

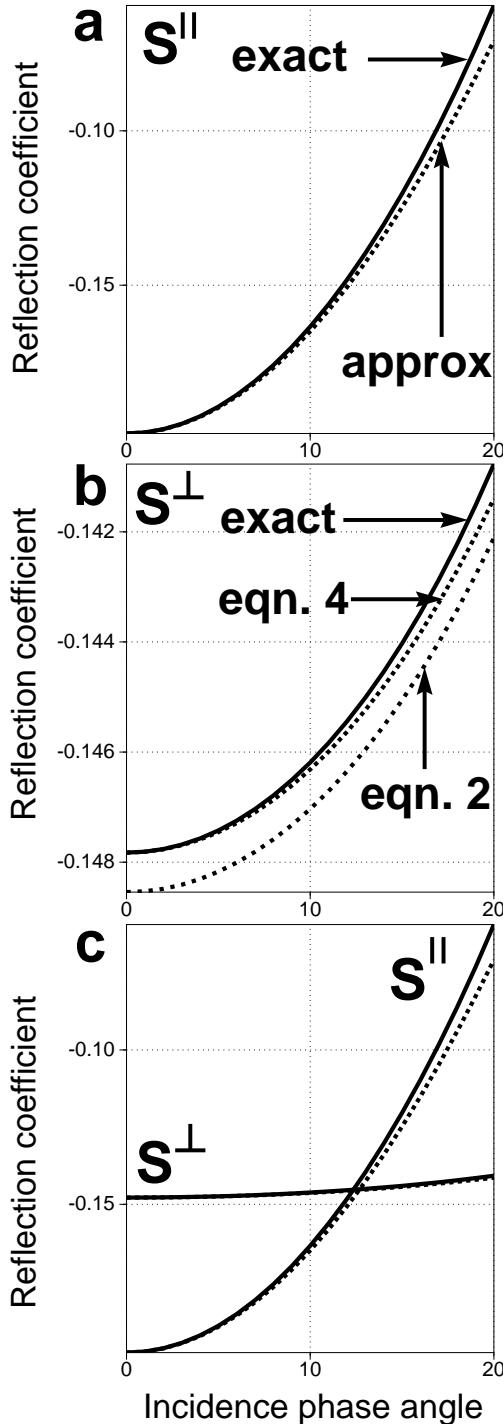


**Figure 5.** Reflection coefficients of shear waves propagating in the isotropy plane. The black curves denote the exact solutions. Approximations are shown as dashed lines. The upper medium is isotropic, the lower medium has HTI symmetry with the shear-wave splitting parameter  $\gamma = 0.115$ ; the vertical  $P$  and  $S^{\parallel}$ -wave velocities of the lower medium are 2.69 km/s and 1.4 km/s; its density is 2.07 g/cm<sup>3</sup>. A relative change of 20 percent in the vertical compressional velocity, vertical  $S^{\parallel}$ -wave velocity and density across the reflecting boundary are assumed. To better recognize differences between the  $S^{\parallel}$  and  $S^{\perp}$  coefficients, the first two plots are combined and shown in the lower figure.

### Symmetry-line survey

Let us now consider a survey line acquired along the axis of symmetry (the  $x_1$ -axis in Figure 4). As discussed in the last section, wave propagation in the symmetry-axis plane is more complicated than in the fracture plane. Fortunately, the derivations necessary for this study are rather straightforward if one applies the analogy between elastic wave propagation in the  $[x_1, x_3]$  plane of HTI and VTI models, first recognized by Rüger (1996a) and Tsvankin (1996c).

Propagation of body waves in elastic media is governed by the Christoffel matrix, here shown in the  $c_{ijkl}$ -tensor notation with slowness components  $p_i$ :

$$\det |c_{ijkl} p_j p_l - \rho| = 0 \quad (13)$$

Using the Voigt recipe to compact the indices of the fourth-order tensor  $c_{ijkl}$  (Musgrave, 1970), equation (13) applied to wave propagation in the  $[x_1, x_3]$  plane of HTI media with the symmetry axis pointing in the  $x_1$  direction takes the form

$$0 = (c_{55} p_1^2 + c_{44} p_3^2 - \rho) \times \begin{vmatrix} c_{11} p_1^2 + c_{55} p_3^2 - \rho & (c_{13} + c_{55}) p_1 p_3 \\ (c_{13} + c_{55}) p_1 p_3 & c_{33} p_3^2 + c_{55} p_1^2 - \rho \end{vmatrix}. \quad (14)$$

Equation (14) *coincides* with the corresponding equation for the VTI medium with the symmetry axis pointing in the  $x_3$  direction. However, it is crucial to understand that in HTI media  $c_{55} = c_{66}$ , whereas VTI symmetry implies that  $c_{55}$  equals  $c_{44}$ .

The second term of equation (14) provides the solution for the velocities and the polarization direction of  $P$ - and shear waves ( $S^{\perp}$ -wave for HTI models and  $SV$ -wave for VTI media) with polarization vectors confined to the  $[x_1, x_3]$ -plane. Thus, all equations describing velocities, traveltime, polarization and stresses in the  $[x_1, x_3]$ -plane are identical for media with the symmetry axis pointing in either the  $x_1$  (HTI) or the  $x_3$  (VTI) direction.

In other words, for any HTI model there exists an “equivalent” VTI model that has the same kinematic properties and polarizations of  $P$  and  $S^{\perp}$  waves in the  $[x_1, x_3]$ -plane. Thus,  $P$ - and  $S^{\perp}$ -wave propagation in the  $[x_1, x_3]$ -plane of HTI media can be described by the known VTI equations using the elastic stiffness components  $c_{ij}$  or, alternatively, using Thomsen’s parameters  $\epsilon^{(V)}$  and  $\delta^{(V)}$  defined for the equivalent VTI model (Rüger, 1996a; Tsvankin, 1996c):

$$\begin{aligned} \gamma^{(V)} &\equiv \frac{c_{66} - c_{44}}{2c_{44}} \\ \epsilon^{(V)} &\equiv \frac{c_{11} - c_{33}}{2c_{33}} \\ \delta^{(V)} &\equiv \frac{(c_{13} + c_{55})^2 - (c_{33} - c_{55})^2}{2c_{33}(c_{33} - c_{55})}. \end{aligned} \quad (15)$$

The coefficients  $\epsilon^{(V)}$  and  $\delta^{(V)}$  can be expressed through the generic Thomsen parameters  $\gamma$ ,  $\epsilon$  and  $\delta$  as defined with respect to the horizontal symmetry axis in the following way:

$$\begin{aligned}\gamma^{(V)} &= -\frac{\gamma}{1+2\gamma} \\ \epsilon^{(V)} &= -\frac{\epsilon}{1+2\epsilon} \\ \delta^{(V)} &= \frac{\delta - 2\epsilon \left(1 + \frac{\epsilon}{f}\right)}{(1+2\epsilon) \left(1 + \frac{2\epsilon}{f}\right)},\end{aligned}\quad (16)$$

where

$$f \equiv 1 - (\beta_0/\alpha_0)^2,$$

as introduced in Tsvankin (1996b). Both  $\alpha_0$  and  $\beta_0$  are measured along the horizontal symmetry axis.

Recognizing this analogy between VTI and HTI models has broad implications and can be used to solve the reflection/transmission problem in the symmetry-axis plane. Note that the boundary conditions are identical for the VTI and the HTI model since in both cases, the incident waves are reflected from the  $[x_1, x_2]$  plane resulting in the identical expressions for the tractions and displacements at the boundary. Consequently, the exact analytic solution for the VTI reflection problem (Graebner, 1992) is valid for reflection coefficients in HTI media, as long as the incident wave is confined to the symmetry-axis plane. Moreover, this solution is also valid for interfaces between VTI and HTI media, no matter whether the HTI medium is above or below the boundary.

This limited analogy between VTI and HTI media can be applied to obtain the approximate reflection coefficient  $R_{S^\perp}^{\text{sym}}$  from equation (8):

$$\begin{aligned}R_{S^\perp}^{\text{sym}} &= R_{S^\perp}^{\text{iso}} + 1/2 \left(\frac{\bar{\alpha}}{\beta^\perp}\right)^2 \times \\ &\quad (\epsilon_2^{(V)} - \epsilon_1^{(V)} + \delta_1^{(V)} - \delta_2^{(V)}) \sin^2 j,\end{aligned}\quad (17)$$

with  $\beta$  in  $R_{S^\perp}^{\text{iso}}$  denoting  $\beta^\perp$ , the vertical velocity of the shear wave polarized in the symmetry-axis plane.

Very similar arguments allow to obtain the reflection coefficient for the  $S^\parallel$  wave. The only additional information required is that in VTI media,  $c_{44}$  equals  $c_{55}$ , whereas in HTI media,  $c_{55}$  equals  $c_{66}$ . The approximate reflection coefficient then yields:

$$R_{S^\parallel}^{\text{sym}} = R_{S^\parallel}^{\text{iso}} + 1/2 (\gamma_2^{(V)} - \gamma_1^{(V)}) \tan^2 j. \quad (18)$$

Here, the  $\beta$ -term in  $R_{S^\parallel}^{\text{iso}}$  corresponds to the vertical  $S^\parallel$  wave-velocity. Figure 6 shows the symmetry-axis-plane reflection coefficients for the same model as in Figure 5. Again, the accuracy of the approximations is sufficiently high for both shear modes. The approximation for the  $S^\perp$  virtually coincides with the exact solution. Also note

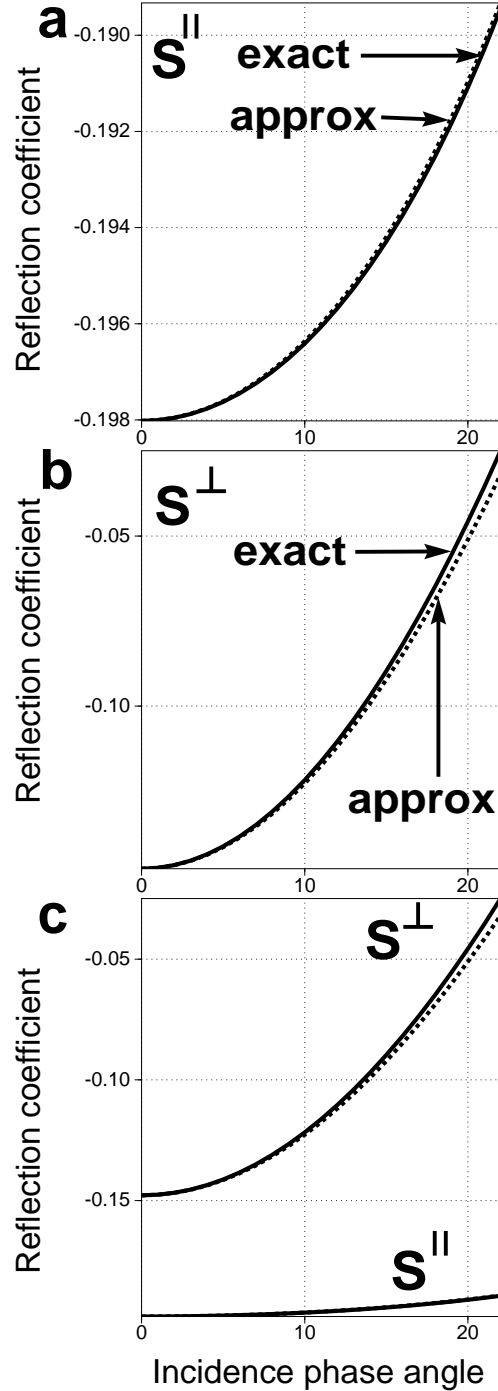


**Figure 6.** Symmetry-axis plane reflection coefficients for both shear modes. Exact solutions are shown as black lines. The model is identical to the one used to generate the reflection coefficients in Figure 5. The anisotropy parameters of the lower medium are  $\gamma^{(V)} = -0.093$  ( $\gamma = 0.115$ ),  $\epsilon^{(V)} = -0.109$  and  $\delta^{(V)} = -0.154$ . The upper medium is purely isotropic.

the significant differences in the gradient and intercept of the reflection responses of the two individual shear modes. Ignoring anisotropy (and assuming that  $\beta$  is the shear velocity in the lower medium) would result in over-estimated AVO gradients and a zero difference in normal-incidence reflection coefficients.

### Dependence on the shear-wave splitting parameter

The application of the developed analytic results requires finding a set of parameters suitable for comparison of the individual shear-wave reflection coefficients. Obviously, for anisotropic media,  $\beta (\doteq \beta^{\parallel}) \neq \beta^{\perp}$ . The parameter of most interest in reservoir characterization is the crack density that is proportional to the product of the number of cracks per unit volume and their mean cubed diameter. Since the crack density for penny-shaped cracks is close to the shear-wave splitting parameter  $\gamma$  (Tsvankin, 1996c), I will retain  $\gamma$  in the expressions for both shear waves. From the definition of anisotropy parameter  $\gamma$ , it follows that

$$\begin{aligned} \beta^{\perp} &= \frac{\beta}{\sqrt{1+2\gamma}} \approx \beta(1-\gamma), \\ \frac{\Delta\beta^{\perp}}{\beta^{\perp}} &\approx \frac{\Delta\beta}{\beta} + \gamma_1 - \gamma_2, \end{aligned} \quad (19)$$

accurate to first order in  $\gamma$ .  $\frac{\Delta\beta}{\beta}$  will denote the relative change in fast shear-wave velocity for the remainder of this paper. To better understand the accuracy of this approximation, I compute  $\frac{\Delta\beta^{\perp}}{\beta^{\perp}}$  as a function of  $\gamma$  (the upper medium is isotropic) for two values of  $\frac{\Delta\beta}{\beta}$  (Figure 7). Shown are the exact solutions (solid lines) and the approximations based on equation (19). For increasing  $\gamma$ , the contrast in  $\beta^{\perp}$  decreases because the velocity for shear waves polarized perpendicular to the fractures decreases. The approximations show little deviation from the exact result. However, even this small deviation can have an observable influence on the reflection coefficient. Note that the reflection response is formed by small differences in the elastic constants across a boundary and that inaccuracies of the size observed in Figure 7 can be significant.

Using the relation between the vertical shear velocities shown in equation (19), both reflection coefficients for shear waves traveling in the fracture plane [equations (17) and (18)] can be conveniently expressed as follows:

$$\begin{aligned} R_{S^{\parallel}}^{\text{strike}} &= -1/2 \frac{\Delta Z}{Z} \\ &+ \left( \frac{7}{2} \frac{\Delta\beta}{\beta} + 2 \frac{\Delta\rho}{\rho} \right) \sin^2 j \end{aligned}$$

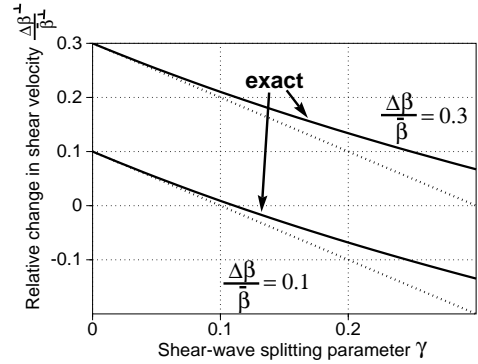


**Figure 7.** Relative change in  $\beta_{S^{\perp}}$  as a function of  $\gamma$  (the upper medium is isotropic) for two values of  $\frac{\Delta\beta}{\beta}$ . Shown are the exact relations (solid lines) and approximations from equation (19) (dashed).

$$\begin{aligned} R_{S^{\perp}}^{\text{strike}} &= -1/2 \frac{\Delta\beta}{\beta} \sin^2 j \tan^2 j \\ &- 1/2 \left( \frac{\Delta Z}{Z} + \gamma_1 - \gamma_2 \right) \\ &+ 1/2 \left( \frac{\Delta\beta}{\beta} + \gamma_1 - \gamma_2 \right) \tan^2 j. \end{aligned} \quad (20)$$

The difference between  $R_{S^{\parallel}}^{\text{strike}}$  and  $R_{S^{\perp}}^{\text{strike}}$  at normal incidence is equal to half the difference in anisotropy across the reflecting interface (Thomsen, 1988). This information can be combined with an estimate of the AVO gradient extracted from the  $S^{\perp}$  data set to yield  $\frac{\Delta\beta}{\beta}$ . The last parameter of interest,  $\frac{\Delta\rho}{\rho}$ , can be calculated from the  $S^{\parallel}$  AVO gradient.

Shear-wave AVO analysis along the strike direction has the potential of uniquely determining the difference in the elastic parameters across a reflecting boundary. In a noisy environment, it may be desirable to further constrain the inversion by adding additional information. A similar analysis, for example, is possible with the higher-angle ( $\sin^2 j \tan^2 j$ ) term, but it is unlikely that this coefficient can be reliably extracted from field data; polarization and amplitude distortions for postcritically incident shear waves can prohibit accurate AVO analysis. Another option is AVO analysis of shear waves propagating normal to the fractures. Clearly, for vertical propagation, there is no distinction between wave propagation in the symmetry-axis plane or the fracture plane. However, the AVO gradients in the symmetry-axis plane are different from those in the fracture plane and these variations can be helpful for an inversion of medium parameters. Taking into account that for weak anisotropy  $\gamma^{(V)} \approx -\gamma$  [equation (16)], we find

$$R_{S^{\parallel}}^{\text{sym}} = -1/2 \frac{\Delta Z}{Z}$$

$$\begin{aligned}
 R_{S^\perp}^{\text{sym}} = & +\frac{1}{2} \left( \frac{\Delta\beta}{\beta} + \gamma_1 - \gamma_2 \right) \tan^2 j \\
 & -1/2 \left( \frac{\Delta Z}{Z} + \gamma_1 - \gamma_2 \right) \\
 & + \left\{ \frac{7}{2} \left( \frac{\Delta\beta}{\beta} + \gamma_1 - \gamma_2 \right) + 2 \frac{\Delta\rho}{\rho} + \right. \\
 & \left. 1/2 \left( \frac{\bar{\alpha}}{\beta} \right)^2 (\epsilon_2^{(V)} - \epsilon_1^{(V)} + \delta_1^{(V)} - \delta_2^{(V)}) \right\} \sin^2 j \\
 & -1/2 \left( \frac{\Delta\beta}{\beta} + \gamma_1 - \gamma_2 \right) \sin^2 j \tan^2 j \quad (21)
 \end{aligned}$$

If the difference  $(\gamma_1 - \gamma_2)$  is extracted from the normal-incidence reflection coefficients, the AVO gradient of the  $S^\parallel$ -wave then provides an additional measure of  $\frac{\Delta\beta}{\beta}$ . Unlike the  $S^\parallel$  wave that solely depends on  $\frac{\Delta\beta}{\beta}$  and  $\gamma$ , the  $S^\perp$  wave is additionally influenced by the difference of coefficients  $\delta^{(V)}$  and  $\epsilon^{(V)}$ ,  $(\delta^{(V)} - \epsilon^{(V)})$ , as demonstrated by Tsvankin (1996c), is close to anisotropy coefficient  $\eta$  (Alkhalifah & Tsvankin, 1995) needed for time processing in transversely isotropic media.

Certainly, the additional linearizations used to derive equations (20) and (21) will change the accuracy of the approximation. To study the quality of the approximation and to observe the variations of the reflection coefficients from one symmetry plane to the other, Figure 8 shows  $S^\parallel$  and  $S^\perp$  reflection coefficients for the same model as used for Figures 5 and 6. As discussed above, the approximation for the  $S^\perp$  reflection coefficients slightly deviates from the exact solution at normal incidence due to the inaccurate value of the relative change in  $\beta_{S^\perp}$ .

The reflection coefficient curves look rather similar for both  $S^\parallel$  and  $S^\perp$  waves in Figure 8, an observation consistent with equations (20) and (21). Specifically, in the weak anisotropy limit, both  $R_{S^\perp}^{\text{strike}}$  and  $R_{S^\parallel}^{\text{sym}}$  have the same AVO gradient. The difference in AVO gradient between  $R_{S^\parallel}^{\text{strike}}$  and  $R_{S^\perp}^{\text{sym}}$ , on the other hand, is a function of  $\Delta\gamma$  and  $\Delta\sigma$ .

Reflection coefficients computed for 4 different combinations of isotropic/HTI interfaces are shown in Figure 9, with model parameters given in Table 1. The first model has only one nonzero anisotropy parameter ( $\delta_2^{(V)}$ ). Equations (20) and (21) correctly predict an identical, moderately negative AVO gradient for  $R_{S^\perp}^{\text{strike}}$  and  $R_{S^\parallel}^{\text{sym}}$  and, after some algebra, a more negative  $R_{S^\parallel}^{\text{strike}}$  gradient as compared to  $R_{S^\perp}^{\text{sym}}$ . The accuracy of the approximations is sufficiently high, as it is the case for the other examples. Model b has a zero value of  $\epsilon_2^{(V)}$ , typical for tight formations such as coal layers. Although the  $S^\parallel$  reflection curves are vertically shifted due to the different normal-incidence reflection coefficients, it is still possible

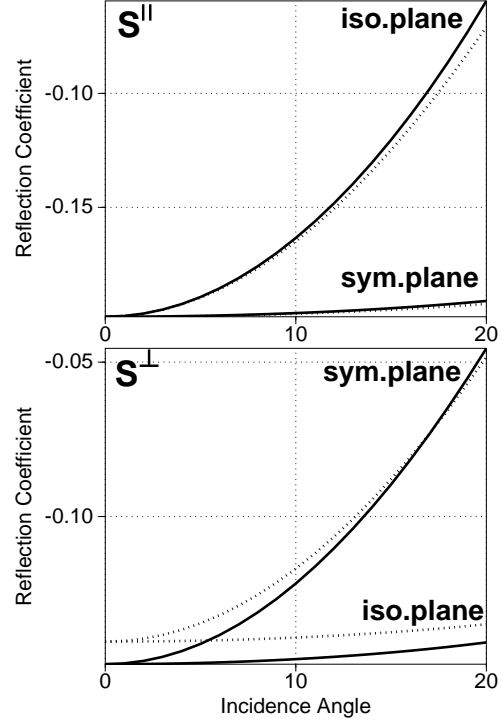


**Figure 8.** Azimuthal variations of  $S^\parallel$  and  $S^\perp$  reflection coefficients for the same model as used for Figures 5 and 6. Shown are exact solutions (solid lines) and approximations based on equation (21)(dashed).

to observe very similar  $R_{S^\perp}^{\text{strike}}$  and  $R_{S^\parallel}^{\text{sym}}$  gradients. The  $R_{S^\perp}^{\text{sym}}$  gradient, on the other hand, is more negative than the  $R_{S^\parallel}^{\text{strike}}$  gradient. The same observation can be made for Model c, with nonzero anisotropy parameter in the lower medium. Finally, a model of elliptical anisotropy ( $d_2^{(V)} = \epsilon_2^{(V)}$ ) is used in example d.

Note that approximations (20) and (21) use the  $S^\parallel$ -wave vertical velocity as parameter, hence the difference in accuracy between the  $S^\parallel$  and  $S^\perp$  coefficients is not related to the physics, but is a matter of design of the approximations. It is straightforward to rewrite equations (20) and (21) as functions of  $\frac{\Delta\beta^\perp}{\beta^\perp}$  if this parameter is better known as compared to  $\frac{\Delta\beta}{\beta}$ .

The examples shown in Figure 9 demonstrate that the derived approximations are accurate for positive and negative jumps in relative difference of the isotropic parameters across the reflecting boundary and nonzero values of anisotropy parameters. Moreover, rather than just studying the AVO gradients for each wavetype independently, equations (20) and (21) motivate to additionally explore the differences in AVO gradients for waves

	Model a	Model b	Model c	Model d
$\frac{\Delta\alpha}{\bar{\alpha}}$	-0.1	0.1	-0.1	0.1
$\frac{\Delta\beta}{\bar{\beta}}$	-0.15	-0.15	-0.1	0.1
$\frac{\Delta\rho}{\bar{\rho}}$	-0.15	-0.15	-0.1	0.1
$\epsilon_2^{(V)}$	0	0	-0.11	-0.11
$\delta_2^{(V)}$	-0.15	-0.067	-0.18	-0.11
$\gamma$	0	0.15	0.15	0.05

**Table 1.** Model parameters for the reflection-coefficient experiments shown in Figure 9. The vertical  $P$  and  $S^{\parallel}$ -wave velocities of the lower medium are 2.69km/s and 1.4km/s; its density is 2.07 g/cm<sup>3</sup>. The upper medium is purely isotropic.

propagating in the vertical symmetry planes of HTI media. Keeping just the lowest-order term and denoting  $\Delta\sigma^{(V)} = \left(\frac{\bar{\alpha}}{\bar{\beta}}\right)^2 (\Delta\epsilon^{(V)} - \Delta\delta^{(V)})$ , we find the following differences in the reflection responses:

$$\begin{aligned}
R_{S^{\parallel}}^{\text{sym}} - R_{S^{\perp}}^{\text{strike}} &= -1/2 \Delta\gamma \\
R_{S^{\parallel}}^{\text{strike}} - R_{S^{\perp}}^{\text{strike}} &= -1/2 \Delta\gamma + \\
&\quad \left(3 \frac{\Delta\beta}{\bar{\beta}} + 2 \frac{\Delta\rho}{\bar{\rho}} + 1/2 \Delta\gamma\right) \sin^2 j \\
R_{S^{\perp}}^{\text{sym}} - R_{S^{\parallel}}^{\text{strike}} &= 1/2 \Delta\gamma + \\
&\quad (-7/2 \Delta\gamma + 1/2 \Delta\sigma^{(V)}) \sin^2 j \\
R_{S^{\parallel}}^{\text{sym}} - R_{S^{\parallel}}^{\text{strike}} &= -\left(3 \frac{\Delta\beta}{\bar{\beta}} + 2 \frac{\Delta\rho}{\bar{\rho}} + 1/2 \Delta\gamma\right) \sin^2 j \\
R_{S^{\perp}}^{\text{sym}} - R_{S^{\perp}}^{\text{strike}} &= \left(3 \left(\frac{\Delta\beta}{\bar{\beta}} - \Delta\gamma\right) + 2 \frac{\Delta\rho}{\bar{\rho}} + \right. \\
&\quad \left. 1/2 \Delta\sigma^{(V)}\right) \sin^2 j \\
R_{S^{\parallel}}^{\text{sym}} - R_{S^{\perp}}^{\text{sym}} &= -1/2 \Delta\gamma - \left(3 \left(\frac{\Delta\beta}{\bar{\beta}} - \Delta\gamma\right) + \right. \\
&\quad \left. 2 \frac{\Delta\rho}{\bar{\rho}} + 1/2 \Delta\sigma^{(V)}\right) \sin^2 j \quad (22)
\end{aligned}$$

Four different configurations allow to obtain the shear-wave splitting parameter from the difference in normal incidence reflection coefficient. Additionally, 5 equations for the differences in the AVO gradients can be solved for the 4 unknowns  $\frac{\Delta\beta}{\bar{\beta}}$ ,  $\frac{\Delta\rho}{\bar{\rho}}$ ,  $\Delta\gamma$  and  $\Delta\sigma^{(V)}$ .

## Off-symmetry-plane polarization

The reflection coefficients discussed so far correspond to the two vertical symmetry planes of HTI media. In principle, it is possible to derive off-symmetry reflection responses for the individual wave types in the same manner as outlined by (Thomsen, 1993) and (Rüger, 1996a), but it is doubtful if the resulting expressions would be usable in practice. Interpretation of shear-wave data for waves with polarizations vectors outside the two vertical symmetry planes is very complicated even in the case of a reflection from an isotropic/isotropic interface: shear waves with nonzero polarization components perpendicular and parallel to the incidence plane will get rotated upon reflection due to the different reflection coefficients for the two components.

A simple isotropic layer on top of a reflecting azimuthally anisotropic medium will cause a rotation of the polarization vector even if the shear-wave polarization is aligned or perpendicular to the incidence plane. Consider the shear-wave displacement vector shown in plane view in Figure 10. This vector can be decomposed in two components parallel and perpendicular to fracture strike. Upon incidence on the reflecting HTI boundary, both components are scaled by individual reflection coefficients and SV/SH conversions are generated. Although the reflected shear wave is *not* split in a fast and slow component, the difference in reflection coefficient will effectively yield a rotation of the polarization vector. The resulting amplitude will be a composite of the reflection response for the parallel and perpendicular components. Although this amplitude and the rotation angle contain information about the anisotropy in the lower layer, this information is hard to extract and thus severely hampers any reliable AVO study.

## Propagation in anisotropic overburden

The goal of AVO analysis is to investigate the angular variation of reflection coefficients rather than directly studying the change of amplitudes with offset. As mentioned above, a substantial amplitude distortion may be associated with wave propagation in anisotropic layers above the reflector. To obtain the reflection coefficients at the target horizon, it is necessary to correct for the amplitude variation associated with the wave propagation between the reflector and the surface. Specifically, the presence of anisotropy in the overlying medium leads to wavefront focusing phenomena, i.e., distortions of the amplitude distribution along the wavefronts of the incident and reflected waves (Tsvankin, 1995). One example herefore can be seen in Figure 3d, where the areas of high

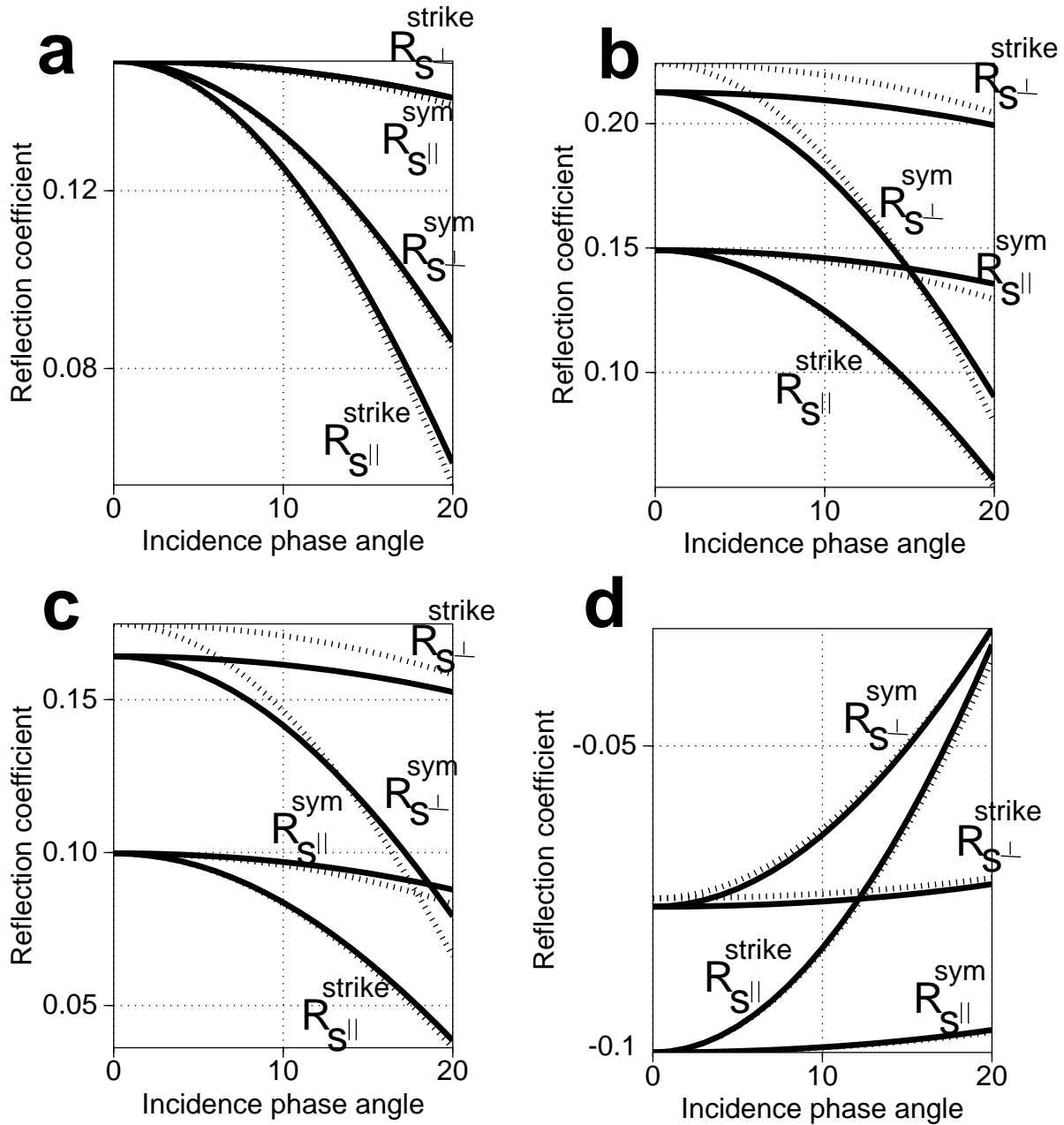


**Figure 9.**  $S^{\parallel}$  and  $S^{\perp}$  reflection coefficients for the two vertical symmetry planes at isotropic/HTI interfaces. Shown are exact solutions (solid lines) and approximations based on equation (20) and (21) (dashed). The model parameters are given in Table 1.

concentration of ray vectors indicate focusing of energy along the wavefront.

The presence of anisotropy in the overburden may be quite typical for fractured reservoirs. Examples of a VTI-HTI boundary include shale-sandstone interfaces such as those discussed by Haugen (1996); also, it is quite com-

mon that fracturing extends throughout the section, making the overburden azimuthally anisotropic.

$P$ - and  $S$ -wave radiation patterns from point sources in VTI media derived in Tsvankin (1995) show that anisotropy has a comparable influence on both energy focusing and the reflection coefficient. The angular amp-

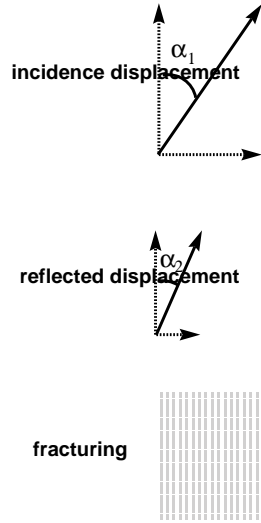


**Figure 10.** Displacement components parallel and to the fracturing (shown in plane view) are scaled with different reflection coefficients, causing a rotation of the polarization angle.

litude dependence of  $P$  waves in the symmetry-axis plane of HTI media has been described by Rüger and Tsvankin (1995). The corresponding results for  $S^{\parallel}$  and  $S^{\perp}$  waves are

$$U_{S^{\perp}}(R, \theta) = \frac{F_u}{4\pi\rho^{(1)}b_0^2 R} (1 - \sigma_1 + 2\sigma_1 \sin^2 2\theta - \sigma_1 \sin^2 \theta), \quad (23)$$

with  $\sigma_1 = \left(\frac{\alpha_0}{\beta_0}\right)^2 (\epsilon_1 - \delta_1)$ , and

$$U_{S^{\parallel}}(R, \theta) = \frac{F_u}{4\pi\rho^{(1)}b_0^2 R} (1 - \gamma_1 - \gamma_1 \sin^2 \theta), \quad (24)$$

where  $U$  is the magnitude of the displacement,  $\rho^{(1)}$  is the density and  $\alpha_0$  and  $b_0$  are the compressional and shear-wave symmetry-direction velocities in the incidence medium.  $R$  is the source-receiver distance and the source term  $F_u$  is the projection of the force on the displacement (polarization) vector. The wavefront focusing [equations (23) and (24)] and the reflection coefficients [equations (21)] have comparable impacts on angular amplitude variations. Equation (23) predicts a sharp increase of amplitude away from vertical with a maximum at about  $40^\circ$  for typical positive values of  $\sigma$ . As expected from Figure 3c, the focusing is much less severe for the  $S^{\parallel}$  wave and the  $S^{\parallel}$  displacement magnitude smoothly decays for increasing angle with vertical.

### Constraining the inversion for anisotropy parameters

Analysis of AVO intercepts and gradients of the individual shear waves can be combined with a study of

the differences in the reflection coefficients in the symmetry planes as indicated in equations (22). Certainly, for high-quality surveys these data are sufficient to solve for the change in isotropic medium parameters as well as for anisotropy parameters  $\gamma$  and  $\sigma$  in the subsurface. In more realistic situations, amplitude extraction from shear-wave data is a difficult task and it is useful to combine all additionally available data for a robust inversion of the medium parameters.

The conventional method of determining  $\gamma$  from surface data is based on analyzing the differences in traveltime between vertically traveling  $S^{\perp}$  and  $S^{\parallel}$  waves (Crampin, 1985) and comparison of normal-incidence reflection coefficients. More recently, Rüger and Tsvankin (1995) described an algorithm to obtain estimates of  $\gamma$  and  $\delta^{(V)}$  from  $P$ -wave AVO analysis.

An alternative approach to constrain the inversion is to use the azimuthal variations in the normal-moveout velocities in HTI media. Normal-moveout velocities from horizontal reflectors in HTI media have been derived by Tsvankin (1996c). Here, I show the linearized expressions for shear-wave NMO velocities in the vertical symmetry planes:

$$\begin{aligned} V_{\text{nmo}}^{\text{strike}} [P - \text{wave}] &= \alpha \\ V_{\text{nmo}}^{\text{strike}} [S^{\perp} - \text{wave}] &= \beta^{\perp} \\ V_{\text{nmo}}^{\text{strike}} [S^{\parallel} - \text{wave}] &= \beta, \end{aligned} \quad (25)$$

and

$$\begin{aligned} V_{\text{nmo}}^{\text{sym}} [P - \text{wave}] &\approx \alpha (1 + \delta^{(V)}) \\ V_{\text{nmo}}^{\text{sym}} [S^{\perp} - \text{wave}] &\approx \beta^{\perp} (1 + \sigma^{(V)}) \\ V_{\text{nmo}}^{\text{sym}} [S^{\parallel} - \text{wave}] &\approx \beta (1 - \gamma). \end{aligned} \quad (26)$$

Equations (25) and (26) indicate that the azimuthal variation of NMO velocity can be inverted for anisotropy parameters. For example, a simple method to estimate  $\gamma$  is to study the  $S^{\parallel}$ -wave NMO velocity perpendicular and parallel to fracture strike (Tsvankin, 1996c). The difference in NMO velocity is close to the shear-wave splitting parameter  $\gamma$ . Unlike the purely hyperbolic moveout of  $S^{\parallel}$ -wave reflections from horizontal interfaces, the moveout of  $P$  and  $S^{\perp}$  waves deviates from a hyperbola even for a single horizontal layer in homogeneous HTI media. However, the deviations in the symmetry-axis plane are small for most realistic values of anisotropy and conventional spread lengths (Tsvankin & Thomsen, 1994).

If the medium is stratified and composed of transversely isotropic layers, the azimuthal NMO analysis is still possible in through-going symmetry-planes using the generalized Dix equation presented by Alkhalifah and Tsvankin (1995). Thus, even if the vertical resolution is smaller for the study of kinematic signatures, it is cer-

tainly beneficial to combine moveout and AVO analysis to obtain a more stable inversion.

The most likely application of the developed methodology is in seismic investigations of fractured reservoirs. The derived equations, however, are valid for HTI media of any origin. If the symmetry is created by thin layering or thin vertical cracks, only two of the three anisotropy parameters are independent, further simplifying the inversion.

### Orthorhombic media

HTI media are useful models to study the first-order influence of azimuthal anisotropy. For cracked media, any deviation from vertical penny-shaped cracks embedded in an isotropic matrix requires the investigation of models with lower symmetry. Media of orthorhombic symmetry, for example, are believed to describe more realistic models of fractured reservoirs such as layers with swarms of elongated cracks. The orthorhombic symmetry system includes azimuthally anisotropic strata caused by a combination of horizontal layering and vertically aligned cracks. Orthorhombic symmetry can also be created by a system of two orthogonal but not necessary identical crack systems or two indistinguishable crack systems at oblique angle (Winterstein, 1990).

The derivations of HTI and orthorhombic media reflection coefficients are very similar. Analysis of symmetry-plane Christoffel systems yields the scattering coefficients and naturally leads to the introduction of a new effective parameterization (Tsvankin, 1996a). For completeness, I state the  $[x_1, x_3]$ -symmetry-plane reflection coefficients for the shear wave polarized (for vertical incidence and symmetry-plane propagation) in the  $[x_1, x_3]$ -plane ( $S^\perp$ ), and in the  $[x_2, x_3]$ -plane ( $S^\parallel$ ):

$$\begin{aligned} R_{S^\parallel}^{[x_1, x_3]} &= R_{SH}^{\text{iso}} + \\ &\quad 1/2 (\gamma_2^{(2)} - \gamma_1^{(2)}) \tan^2 j \\ R_{S^\perp}^{[x_1, x_3]} &= R_{SV}^{\text{iso}} + 1/2 \left( \frac{\bar{\alpha}}{\beta^\perp} \right)^2 \times \\ &\quad (\epsilon_2^{(2)} - \epsilon_1^{(2)} + \delta_1^{(2)} - \delta_2^{(2)}) \sin^2 j, \end{aligned} \quad (27)$$

with shear-wave velocities  $\beta = \sqrt{c_{44}/\rho}$  in  $R_{S^\parallel}^{[x_1, x_3]}$  and  $\beta^\perp = \sqrt{c_{55}/\rho}$  in  $R_{S^\perp}^{[x_1, x_3]}$ . Parameters  $\delta^{(2)}$  and  $\epsilon^{(2)}$  are responsible for near-vertical and near-horizontal  $P$ -wave propagation, respectively, exactly as  $\delta$  and  $\epsilon$  in VTI models.  $\gamma^{(2)}$  determines the velocity variation of the  $S^\parallel$  wave polarized normal to the  $[x_1, x_3]$ -plane.

For shear waves propagating in the  $[x_2, x_3]$ -plane, the

Orthorhombic	VTI	HTI
$\delta^{(2)} = \frac{(c_{13}+c_{55})^2 - (c_{33}-c_{55})^2}{2c_{33}(c_{33}-c_{55})}$	$\delta$	$\delta^{(V)}$
$\delta^{(1)} = \frac{(c_{23}+c_{44})^2 - (c_{33}-c_{44})^2}{2c_{33}(c_{33}-c_{44})}$	$\delta$	0
$\epsilon^{(2)} = \frac{c_{11}-c_{33}}{2c_{33}}$	$\epsilon$	$\epsilon^{(V)}$
$\epsilon^{(1)} = \frac{c_{22}-c_{33}}{2c_{33}}$	$\epsilon$	0
$\gamma^{(2)} = \frac{c_{66}-c_{44}}{2c_{44}}$	$\gamma$	$\gamma^{(V)}$
$\gamma^{(1)} = \frac{c_{66}-c_{55}}{2c_{55}}$	$\gamma$	0

**Table 2.** Anisotropy parameters describing orthorhombic anisotropy. Their relations to generic (VTI) Thomsen coefficients and to HTI parameters  $\delta^{(V)}$ ,  $\gamma^{(V)}$  and  $\epsilon^{(V)}$  are shown in the second and third column.

solutions for the reflection coefficients are as follows:

$$\begin{aligned} R_{S^\parallel}^{[x_2, x_3]} &= R_{SH}^{\text{iso}} + 1/2 \left( \frac{\bar{\alpha}}{\beta} \right)^2 \times \\ &\quad (\epsilon_2^{(1)} - \epsilon_1^{(1)} + \delta_1^{(1)} - \delta_2^{(1)}) \sin^2 j. \\ R_{S^\perp}^{[x_2, x_3]} &= R_{SV}^{\text{iso}} + \\ &\quad 1/2 (\gamma_2^{(1)} - \gamma_1^{(1)}) \tan^2 j. \end{aligned} \quad (28)$$

As before, the  $S^\parallel$ -wave coefficients are shown with velocity  $\beta$  whereas the  $S^\perp$ -wave vertical shear-velocity is  $\beta^\perp$ . A definition of the new effective coefficients and their relations to the generic Thomsen parameters (VTI) and HTI parameters is given in Table 2. Note that the conventionally studied shear-wave splitting parameter  $\gamma^{(s)} \doteq \frac{c_{44}-c_{55}}{2c_{55}} = \frac{\gamma^{(1)}-\gamma^{(2)}}{1+2\gamma^{(2)}}$  (Tsvankin, 1996a).

### Conclusions

If the shear-wave AVO gradients can be reliably extracted from prestack shear-wave amplitudes, they can supplement the fracture-detection algorithm based on the normal-incidence shear-wave reflection coefficients (Thomsen, 1988; Mueller, 1991).

This paper elucidates the physics of energy-partitioning of shear waves in azimuthally anisotropic media. For the two vertical symmetry planes in HTI symmetry systems, concise analytic expressions of the AVO gradients predict that differences in the shear-wave splitting parameter and anisotropy parameters  $\sigma^{(V)}$  across a reflecting boundary have a first-order influence on shear-wave AVO gradients. AVO gradients for  $S^\parallel$  waves traveling in the symmetry-axis plane and  $S^\perp$  waves propagating along fracture strike are shown to be approximately identical while difference in  $S^\parallel$ -strike and  $S^\perp$ -symmetry axis AVO gradients depends on a weighted sum of  $\gamma$

and  $\sigma^{(v)}$ . Rather than just studying the AVO gradients for each wavetype independently, this analysis suggests to additionally explore the differences in AVO gradients for waves propagating in the vertical symmetry planes of HTI media.

Obviously, amplitude analysis of shear-wave data is a difficult task in realistic settings. To stabilize the inversion algorithm based on shear-wave AVO analysis, I suggest combining the amplitude analysis with a study of the azimuthal variations in normal-moveout velocities. Also, since the magnitude of the splitting parameter is relatively small, even a substantial percentage error in  $\gamma$  may not prevent this algorithm from detecting anomalies in the crack density.

Probably the most restricting assumption in this study is that the symmetry-axis direction has to be known prior to the shear-wave acquisition. If the excited shear-wave polarization is oblique to the natural coordinate system of the subsurface, the reflected shear-wave amplitudes and polarization will be distorted and severely hampers the AVO analysis. Fortunately, for fractured reservoirs, the crack orientation and thus the symmetry axis direction can often be obtained from stress measurements, geologic information and borehole data (e.g., tiltmeter, breakouts) and shear-wave polarization analysis.

Finally, as for  $P$ -wave studies, an essential part of the shear-wave AVO is the correction for energy focusing and defocusing for waves propagating in the anisotropic overburden.

## Acknowledgments

Thanks to Ilya Tsvankin, John Stockwell and Konstantin Osypov for the review of this paper and to members of the A(nisotropy)-Team at the Center for Wave Phenomena (CWP) for useful discussions. The support for this work was provided by the members of the Consortium Project on Seismic Inverse Methods for Complex Structures at CWP, Colorado School of Mines, and by the United States Department of Energy (project "Velocity Analysis, Parameter Estimation, and Constraints on Lithology for Transversely Isotropic Sediments" within the framework of the Advanced Computational Technology Initiative). Partial funding for this project has been provided by a scholarship from Phillips Petroleum Co.

## References

Aki, K., & Richards, P. G. 1980. *Quantitative seismology: Theory and methods*. W. N. Freeman & Co.

- Alford, R. M. 1986. Shear data in the presence of azimuthal anisotropy: Dilley, Texas. *In: 56th Annual Internat. Mtg., Soc. Expl. Geophys., Expanded Abstracts*. Soc. Expl. Geophys.
- Alkhalifah, T., & Tsvankin, I. 1995. Velocity analysis for transversely isotropic media. *Geophysics*, **60**, 1550–1556.
- Banik, N. C. 1987. An effective anisotropy parameter in transversely isotropic media. *Geophysics*, **52**(12), 1654–1664.
- Castagna, & Backus, Eds. 1993. *In Offset Dependent Reflectivity: Theory and methods*. SEG.
- Červený, V. 1972. Seismic rays and ray intensities in inhomogeneous anisotropic media. *Geophys. J. R. astr. Soc.*, **29**, 1–13.
- Crampin, Stuart. 1985. Evidence for aligned cracks in the Earth's crust. *First Break*, **3**, 12–15.
- Crampin, Stuart, & Atkinson, Barry K. 1985. Microcracks in the Earth's crust. *First Break*, **3**, 16–21.
- Graebner, M. 1992. Plane-wave reflection and transmission coefficients for a transversely isotropic solid (short note). *Geophysics*, **57**(11), 1512–1519.
- Haugen, G. 1996. AVO-A analysis of a shale over a vertically fractured sandstone. *In: 71WSA*. Soc. Expl. Geophys.
- Henneke, E. G. 1972. Reflection-refraction of a stress wave at a plane boundary between anisotropic media. *J. Acoust. Soc. Am.*, **51**, 210–217.
- Keith, C.M., & Crampin, S. 1977. Seismic body waves in anisotropic media: reflection and refraction at a plane interface. *Geophys. J. R. Astr. Soc.*
- Kendall, R. R. 1995. Modeling and interpreting shear-waves and fracture anisotropy in South-Central Wyoming. *In: 65nd Annual Internat. Mtg., Soc. Expl. Geophys., Expanded Abstracts*. Soc. Expl. Geophys.
- Lynn, H. B., & Thomsen, L. A. 1990. Reflection shear-wave data collected near the principal axes of azimuthal anisotropy. *Geophysics*, **55**(2), 147–156.
- Lynn, H. B. et al. 1995. Seismic characterization of a naturally fractured reservoir. *In: 65nd Annual Internat. Mtg., Soc. Expl. Geophys., Expanded Abstracts*. Soc. Expl. Geophys.
- Michelena, R. J. 1995. Quantifying errors in fracture orientation estimated from surface P-S converted waves. *In: 65nd Annual Internat. Mtg., Soc. Expl. Geophys., Expanded Abstracts*. Soc. Expl. Geophys.
- Mueller, M. 1991. Prediction of lateral variability in fracture intensity using multicomponent shear-wave surface seismic as a precursor to horizontally drilling in Austin Chalk. *Geophys. J. Int.*, **107**, 409–415.
- Musgrave, M. J. P. 1970. *Crystal acoustics*. Holden

- Day, San Francisco.
- Richards, P. G., & Frasier, C. W. 1976. Scattering of elastic waves from depth-dependent inhomogeneities. *Geophysics*, **41**(3), 441–458.
- Rüger, A. 1994. Efficient anisotropic raytracing. *Proceedings of 6IWSA, special SEG volume on seismic anisotropy, Trondheim, accepted*.
- Rüger, A. 1996a. P-wave reflection coefficients for transversely isotropic models with vertical and horizontal axis of symmetry. *Geophysics*, *submitted*.
- Rüger, A. 1996b. Variation of P-wave reflectivity with offset and azimuth in anisotropic media. *CWP-203 (This volume)*.
- Rüger, A., & Tsvankin, I. 1995. Azimuthal variation of AVO response for fractured reservoirs. *Pages 1103–1106 of: 65th Annual Internat. Mtg., Soc. Expl. Geophys., Expanded Abstracts*, vol. 95.
- Shuey, R. T. 1985. A simplification of the Zoeppritz-equations. *Geophysics*, **50**(4), 609–614.
- Thomsen, L. 1986. Weak elastic anisotropy. *Geophysics*, **51**(10), 1954–1966.
- Thomsen, L. 1988. Reflection seismology over azimuthally anisotropic media. *Geophysics*, **53**(3), 304–313.
- Thomsen, L. 1993. Weak anisotropic reflections. *In Offset Dependent Reflectivity (Castagna and Backus, Eds.), SEG, Tulsa*.
- Thomsen, L. 1995. Elastic anisotropy due to aligned cracks in porous rock. *Geophysical Prospecting*, **43**, 805–829.
- Tsvankin, I. 1995. Body-wave radiation patterns and AVO in transversely isotropic media. *Geophysics*, **60**(5), 1409–1425.
- Tsvankin, I. 1996a. Effective parameters and reflection seismic signatures for orthorhombic anisotropy. *in Center for Wave Phenomena report CWP-199*.
- Tsvankin, I. 1996b. P-wave signatures and notation for transversely isotropic media: An overview. *Geophysics*, **61**(2), 467–483.
- Tsvankin, I. 1996c. Reflection moveout and parameter estimation for horizontal transverse isotropy. *Geophysics*, *accepted*.
- Tsvankin, I., & Chesnokov, E. 1990. Synthesis of body-wave seismograms from point sources in anisotropic media. *J. Geophys. Res.*, **95**.
- Tsvankin, I., & Thomsen, L. 1994. Nonhyperbolic reflection moveout in anisotropic media. *Geophysics*, **59**(8), 1290–1304.
- Winterstein, D.F. 1990. Velocity anisotropy terminology for geophysicists. *Geophysics*, **55**, 1070–1088.
- Wright, J. 1986. Reflection coefficients at pore-fluid contacts as a function of offset (short note). *Geophysics*, **51**(9), 1858–1860.
- Yardley, G. S.; Graham, G., & Crampin, S. 1991. Viability of shear-wave amplitude versus offset studies in anisotropic media. *Geophys. J. Int.*, **107**, 493–503.

